Environmental Science Nano

PAPER

Cite this: *Environ. Sci.: Nano*, 2016, **3**, 462

Role of the capping agent in the interaction of hydrophilic Ag nanoparticles with DMPC as a model biomembrane†

Julie V. Maya Girón,[a] Raquel V. Vico,*[b] Bruno Maggio,[c] Eugenia Zelaya,[d] Aldo Rubert,[a] Guillermo Benítez,[a] Pilar Carro,[e] Roberto C. Salvarezza[a] and María E. Vela*[a]

Received 15th January 2016,
Accepted 11th March 2016

DOI: 10.1039/c6en00016a

rsc.li/es-nano

The interaction of 1,2-dimyristoyl-*sn*-glycero-3-phosphocholine (DMPC) Langmuir monolayers as a model biomembrane with small silver nanoparticles (AgNPs) similar in size but coated with different capping molecules such as citrate (CIT-AgNPs) and 4-mercaptobenzoic acid (MBA-AgNPs), both negatively charged at physiological pH, is studied using a multi-technique approach. Both CIT-AgNPs and MBA-AgNPs expose carboxyl groups and have similar zeta potentials, but differ in the aliphatic or aromatic nature of the capping agent. Results show that AgNPs exhibit quite different behaviors: CIT-AgNPs weakly adsorb on DMPC, while MBA-AgNPs irreversibly adsorb on the interface and remain there upon monolayer compression. It is also shown that there is a cooperative effect of many ligands in the interactions between MBA-AgNPs and DMPC, as MBA molecules in solution are unable to strongly adsorb on the phospholipid monolayer surface. We propose an explanation based on the surface charge density and on the chemical nature of the capping molecule based on XPS studies and on DFT calculations.

Nano impact

Comprehension of the interactions between silver nanoparticles (AgNPs) and biological matter is imperative given their increasing demand and applications. A relevant topic to be investigated is how the sign and charge density of nanoparticles affect their adhesion and penetration into lipid layers. We show that AgNPs similar in size but coated with different molecules such as citrate (CIT-AgNPs) and 4-mercaptobenzoic acid (MBA-AgNPs), both negatively charged at physiological pH, interact in a different way with DMPC Langmuir monolayers taken as a model biomembrane. These results highlight the importance of understanding, at the molecular level, the interactions between nanomaterials and membranes to assess their potential long-term toxicological effects.

Introduction

Silver nanoparticles (AgNPs) are one of the most widely used nanomaterials in commercial products.[1–4] In the bottom-up approach for synthesis, capping agents of different chemical nature allow the control of the NP morphology, size and coalescence. The capping agent has functional groups that on the one hand are able to strongly interact with Ag, and on the other hand provide the chemical functionality to solubilize the NPs in a given solvent and/or interact specifically according to the application searched for those AgNPs.[5–7] Citrate is one of the most common capping agents commercially available, and Turkevich synthesis is a simple and vastly used method.[8,9] In addition to commercial applications, Ag

[a] *Instituto de Investigaciones Fisicoquímicas Teóricas y Aplicadas (INIFTA), Facultad de Ciencias Exactas, Universidad Nacional de La Plata-CONICET, Sucursal 4 Casilla de Correo 16, (1900) La Plata, Argentina. E-mail: mevela@inifta.unlp.edu.ar; Fax: +54 221 4254642*

[b] *Instituto de Investigaciones en Fisicoquímica de Córdoba (INFIQC-CONICET), Departamento de Química Orgánica, Facultad de Ciencias Químicas, Universidad Nacional de Córdoba, Haya de la Torre y Medina Allende, Ciudad Universitaria, X5000HUA, Córdoba, Argentina. E-mail: rvico@fcq.unc.edu.ar; Fax: +54 351 4334074*

[c] *Centro de Investigaciones en Química Biológica de Córdoba (CIQUIBIC-CONICET), Departamento de Química Biológica, Facultad de Ciencias Químicas, Universidad Nacional de Córdoba, Haya de la Torre y Medina Allende, Ciudad Universitaria, X5000HUA, Córdoba, Argentina*

[d] *CAB-CNEA, Av. Bustillo km 9.5 (R8402AGP), S.C. de Bariloche, Argentina*

[e] *Departamento de Química Física, Instituto de Materiales y Nanotecnología, Universidad de La Laguna, Tenerife, Spain*

† Electronic supplementary information (ESI) available: RMN of pure CIT and MBA, UV-vis spectra of CIT-AgNPs and MBA-NPs, calculation of the MBA/CIT molecular ratio on MBA-AgNPs, Marks model for AgNPs, Gibbs isotherms for MBA-AgNPs, compression isotherms for CIT and MBA as components of the buffer subphase, scheme of the molecular structure of DMPC, BAM images taken for a DMPC monolayer film at 5 mN m^{-1} in contact with phosphate buffer solution at pH 7.2 containing MBA-AgNPs and $\sqrt{3} \times 4$ MBA lattice on Ag(1 1 1). See DOI: 10.1039/c6en00016a

nanoparticles have also been extensively employed due to their plasmonic properties to enhance Raman scattering.[10,11]

Due to the increasing demand for and applications of AgNPs, the understanding of their interactions with biological matter is of outmost importance.[12–14] NP binding, rupture and cell membrane penetration strongly depend on its size, shape, surface charge and surface chemical functionality.[15–18] NPs with dimensions smaller than 5 nm can penetrate cell membranes,[16,19,20] while for larger ones their action occurs primarily through alterations of the membrane structure, which can strongly affect its permeability,[4] the membrane potential[21,22] and its main functions.[23–25] For Au nanoparticles it has been found that by controlling their surface charge density, it is possible to reach a balance between toxicity and cellular uptake.[26] Electrostatic interactions of nanoparticles and lipid bilayers mediate their interaction with biological membranes and their disruption. The uptake process should involve NP adsorption onto the cell surface and then, its internalization.[27,28] Thus, how the sign and charge density of nanoparticles at the molecular level affect their adhesion and penetration into lipid layers is a highly relevant topic to be investigated. Due to the complexity of natural biological membranes, supported lipid monolayers or bilayers are the most common model systems used to study their interactions with biomolecules, nanoparticles, *etc.*[29–32] Another advantageous model to study interactions at nano-biointerfaces is Langmuir monolayers, which avoid the transfer of the biomembrane model to a solid support and allow control of the composition and organization at both the interface and the subphase, thus various factors involved in NP–membrane interactions can be investigated.[33–36] In particular, DMPC is a zwitterionic phospholipid that at room temperature shows a full liquid-expanded phase along the whole Langmuir isotherm and a homogeneous topography in the mesoscale range when inspected by Brewster angle microscopy (BAM).

In this work, we study the interaction of DMPC monolayers with silver NPs similar in size but coated with different molecules such as citrate (CIT-AgNPs) and 4-mercaptobenzoic acid (MBA-AgNPs), both negatively charged at physiological pH. MBA-AgNPs were obtained from CIT-AgNPs by the traditional ligand exchange procedure. High resolution XPS experiments show that citrate is not completely removed from the NP surface, which has an important influence in regard to the interaction with the phospholipid monolayer, as will be explained in the following sections. For simplicity, the acronym MBA-AgNPs will be employed for the AgNPs containing MBA and remnant citrate as capping agents. CIT-AgNPs are one of the most widely used in commercial products and scientific applications, while MBA-AgNPs are a common Raman probe used in sensors based upon surface-enhanced Raman spectroscopy (SERS).[37–44] Both CIT-AgNPs and MBA-AgNPs expose carboxyl groups and have similar zeta potentials, but differ in the aliphatic or aromatic nature of the capping agent. Results show that they exhibit quite different behaviors: CIT-AgNPs weakly adsorb on DMPC, while MBA-AgNPs irreversibly adsorb and remain at the interface upon monolayer compression. It is also shown that there is a cooperative effect of many ligands in the interactions between MBA-AgNPs and DMPC, as MBA molecules in solution (without a silver core) are unable to strongly adsorb on the phospholipid surface. We propose an explanation based on the surface charge density and on the chemical nature of the capping molecule based on XPS studies and DFT calculations.

Experimental

Synthesis of Ag nanoparticles

$AgNO_3$, $NaBH_4$ and trisodium citrate were purchased from Sigma-Aldrich, and aqueous solutions were prepared with Milli-Q water. In the first step for the preparation of the dilute suspension of silver nanoparticles, 10 mL of a 0.25 mM $AgNO_3$ solution was added to 10 mL of 0.25 mM sodium citrate solution under gentle magnetic stirring. After 3 min, 25 μL of a 0.1 M aqueous $NaBH_4$ solution cooled in an ice-water bath was added dropwise. The solution was strongly stirred for 3 min, and its color turned from colorless to yellow. The final Ag concentration in the NP solution is 1.35×10^{-2} mg Ag mL^{-1}. The excess of citrate was extracted by a two-hour dialysis procedure. For the preparation of Ag nanoparticles capped with MBA, the purified citrate-capped AgNPs (CIT-AgNPs) were allowed to react with 1 mM MBA + 0.1 M NaOH in a 10 : 1 ratio (citrate Ag-NPs : MBA solution) in order to introduce the MBA molecules into the capping layer. Finally, after 3 h of reaction, the colloidal suspension of MBA capped Ag nanoparticles (MBA-AgNPs) was again dialyzed for 12 h against pH 7.2 10 mM phosphate buffer solution.

More concentrated solutions of CIT-AgNPs and MBA-AgNPs were obtained by tripling the concentrations of the silver nitrate, sodium citrate, sodium borohydride and 4-mercaptobenzoic acid solutions used for the synthesis procedure described previously/above. Experiments with higher concentrations of NPs could not be carried out due to their coalescence. Citrate and MBA were used as received, and their purity was ascertained by ^1H and ^{13}C NMR (see also ESI,† Fig. S1–S4).

Characterization of CIT-AgNPs and MBA-AgNPs

The micrographs used to analyze the size distribution and structure of CIT-AgNPs and MBA-AgNPs were obtained with a FEI CM200 UT microscope operated at 200 keV and a FEI TECNAI F20 field emission microscope operated at 200 keV.

The species in the surface structure of AgNPs were characterized and quantified by X-ray photoelectron spectroscopy (XPS) using an Al Kα source (XR50, Specs GmbH) and a hemispherical electron energy analyzer (PHOIBOS 100, Specs GmbH). The energy scale was calibrated using two points; one was the Au $4f_{7/2}$ binding energy (BE) of sputter cleaned gold at 84.00 eV and the other was the Cu $2p_{3/2}$ BE: 932.67 eV of copper samples.

The spectra were fitted with the XPSPEAK 4.0 software package, using a Shirley type background and Gaussian–Lorentzian product functions. In the case of S 2p, each

component was fitted with a doublet accounting for the spin–orbit splitting (1.2 eV) with a branching ratio of 0.5. The full width at half-maximum (FWHM) was fixed at 1.1 eV. The C 1s region was fitted with four components, as will be discussed later, corresponding to: (i) C–H bonds and adventitious C, (ii) the alpha carbons of carboxylic groups and/or the alcoholic function in the case of CIT-AgNPs, and (iii) and (iv) carboxylate and carboxylic acid group contributions. The BEs and peak areas were optimized to achieve the best fit.

UV-vis absorption spectra were taken with Perkin Elmer Lambda 25 and Shimadzu UV-1801 spectrophotometers at ambient temperature (23–25 °C) to check the quality and concentration of the AgNPs before starting the experiments and after their immersion in the Langmuir trough to check the degradation processes that may eventually occur.

Monolayers at the air/buffer interface

The phospholipid 1,2-dimyristoyl-*sn*-glycero-3-phosphocholine (DMPC) was purchased from Avanti Polar Lipids (Alabaster, AL). For monolayer studies, a 10 mM phosphate buffer of pH 7.2 was used as the subphase. The buffer solutions were prepared with Milli-Q water.

The monolayers were obtained by using a homemade trough with a control unit (Monofilmmeter Mayer Feintechnik, Göttingen, Germany). The surface and volume of the Teflon trough were 43 cm^2 and 34 mL, respectively. The surface pressure (π) was measured by a platinized-Pt sensing plate using the Wilhelmy method.

The absence of impurities in the subphase was checked before starting each experiment by reducing the available surface area to less than 30% of its original value (from 43 cm^2 to 13 cm^2) allowing enough time (10 min) for the adsorption of possible impurities that might be present in trace amounts in the subphase. Only subphases that did not show changes of surface pressure above ± 0.5 mN m^{-1} in this procedure were used. Before each experiment, the trough was rinsed and wiped clean with 98% ethanol and several times with Milli-Q water. The trough was also cleaned daily with sulfonitric solution (70% H_2SO_4/30% HNO_3) and rinsed with Milli-Q water and phosphate buffer to remove the organic contaminants that may affect the experiments. Special care was taken in the experiments with MBA-AgNPs and MBA solutions due to their possible adsorption in the Langmuir trough. All experiments were performed at 23 ± 1 C°.

Adsorption of AgNPs on the air/buffer interface and interaction with phospholipid monolayers. The adsorption of CIT-AgNPs or MBA-AgNPs from the subphase to the bare air/buffer interface, or to DMPC monolayers, was performed by injections of AgNP solution into the buffer subphase under continuous stirring. Typically, 1.5 mL of AgNP solution, containing 2.02×10^{-2} mg or 6.06×10^{-2} mg of Ag for diluted or concentrated suspensions, was used giving a final AgNP concentration of 2.03×10^{11} NPs mL^{-1} or 6.08×10^{11} NPs mL^{-1} for CIT-AgNPs or MBA-AgNPs, respectively.

To study the interactions between AgNPs and DMPC, the phospholipid monolayer was formed by deposition of a pure DMPC chloroformic solution at the air/buffer interface until the desired value of π was achieved. The initial surface pressures of DMPC (π_o^{DMPC}) studied were 3, 5, 10 and 30 mN m^{-1}. Once 10 minutes after DMPC film formation had elapsed, the AgNP solution was injected into the subphase.

The surface pressure was taken as:

$$\pi = \gamma_0 - \gamma \quad (1)$$

where γ_0 and γ are the surface tension of the air/buffer interface in the absence or in the presence of a surface active agent, respectively.[45]

After injection of the particles into the subphase, in the absence or in the presence of DMPC, changes in surface pressure (π) at constant area were recorded as a function of time until the equilibrium adsorption pressure (π_{eq}) was reached. Once the π_{eq} was achieved, the film formed was compressed to obtain a Langmuir isotherm. The compression rate was 0.4 cm^2 s^{-1}. The Langmuir compression isotherms of the interacting AgNPs/DMPC are reported as surface pressure (π) *vs.* mean molecular area (MMA) plots calculated on the basis of the area that should be occupied by pure DMPC. MMA is the total monolayer area divided by the total number of molecules at the interfaces.

For control purposes, Langmuir isotherms of pure DMPC were obtained by seeding DMPC at the interface until a given surface pressure (*i.e.*, 5, 10, 30 mN m^{-1}) was reached and then, after 10 min, the film was compressed. No differences with the Langmuir isotherm of DMPC starting from the gaseous phase ($\pi \sim 0$ mN m^{-1}) were observed.

Also, either citrate or MBA solutions at concentrations similar to or higher than that provided by the AgNPs were injected into the subphase and then, the π as a function of time as well as the compression isotherms (π *vs.* area) were recorded.

The addition of up to 2 mL of pure buffer to the buffer subphase did not cause any variation in π.

Different batches of both silver nanoparticles were tested, and no differences were observed. In all cases, the triplicate adsorption and compression experiments performed did not vary among them by more than 0.3–0.5 mN m^{-1} (adsorption isotherms) or 5% in area (compression isotherms).

In order to check whether both CIT-AgNPs and MBA-AgNPs undergo any degradation after their adsorption on the bare interface or after their interaction with the DMPC monolayer, the UV-visible spectra of the subphase were measured. For this, an aliquot of the subphase was taken after the adsorption (typically 2 h after the addition of AgNPs) and the UV-visible spectra were compared with that of the freshly prepared AgNPs. No changes in the optical response confirmed that neither coalescence nor degradation take place during the experiments for CIT-AgNPs and MBA-AgNPs (Fig. S5a–b†).

Brewster angle microscopy visualization. For 2D isotropic films, the reflectivity obtained from BAM measurements is

related to the square of the film thickness and to the refraction index of the film.

Adsorption monolayers were prepared by using a circular homemade trough with an area of 28 cm^2 and a subphase volume of 28 mL. The amount of AgNP solution injected into the subphase was 0.5 mL; higher volumes cause higher reflectivities that avoid the proper visualization of the surface. Interaction experiments between AgNPs and DMPC were performed as mentioned in the above section. Brewster angle visualization was performed without stirring to avoid the movement of the films. The trough was mounted on the stage of a Nanofilm EP3 Imaging Ellipsometer (Accurion, Göttingen, Germany), which was used in the BAM mode. The minimum reflection was set with a polarized laser (λ = 532) incident on the bare aqueous surface at the experimentally calibrated Brewster angle (~53.1°). During the adsorption of NPs on the DMPC monolayer, the reflected light was collected through a 20× objective and an analyzer-polarized lens to a CCD camera with a speed of 25 Hz. The surface pressure was measured along time with a KSV platinized-Pt sensing plate using the Wilhelmy method.

Control experiments were performed with citrate and MBA at similar to or higher concentrations than that provided by the AgNPs.

DFT calculations

DFT calculations were performed with the periodic plane-wave basis set code VASP 5.2.12.[46,47] We followed the scheme of nonlocal functionals proposed by Dion *et al.*[48] vdW-DF, and the optimized Becke88 exchange functional optB88-vdW[49] to take into account the van der Waals (vdW) interactions. The electronic wave functions were expanded in a plane-wave basis set with a 450 eV cutoff energy. The projector augmented plane wave (PAW) due to the Blöchl method was used to represent the atomic cores[50] with PBE potential. Silver surfaces were represented by a five atomic layer slab with ~15 Å vacuum. Optimal grids of Monkhorst–Pack[51] *k*-points of 5 × 5 × 1 were used for numerical integration in the reciprocal space of (2√3 × 4) surface structure. Surface relaxation is allowed in the three uppermost Ag layers of the slab as well as in the atomic coordinates of the adsorbate. The citrate radical species (Citrate H^{2-}) was optimized in an asymmetric box of 10 Å × 12 Å × 14 Å. The calculated lattice constant is 4.14 Å, which compares reasonably well with the experimental value (4.09 Å).[52]

The average binding energy per adsorbed citrate radical, E_b, is defined in eqn (2):

$$E_b = \frac{1}{N_{\text{citrate}}}\left[E^{\text{slab+citrate}} - E^{\text{slab}} - N_{\text{citrate}}E^{\text{citrate}}\right] \quad (2)$$

where $E^{\text{slab+citrate}}$, E^{slab} and E^{citrate} are the total energy of the relaxed citrate-surface system, the relaxed bare substrate, and the citrate radical, whereas N_{citrate} is the number of citrate radicals in the surface unit cell. It is necessary to note that a negative number indicates that adsorption is exothermic with respect to the separate clean surface and the citrate radical.

Results and discussion

NP characterization

Typical high resolution TEM (HRTEM) images of fresh MBA-AgNPs and CIT-AgNPs are shown in Fig. 1. The low magnification images in a) and b) show that both NPs are spherically-shaped with average sizes of 8.7 ± 2.5 nm for CIT-AgNPs and 8.2 ± 2.1 nm for MBA-AgNPs, calculated from their corresponding histograms, c) and d). HRTEM images allow the atomic structure of the AgNPs to be resolved (Fig. 1e and f). The images are compatible with the [1 0 0] zone axis and the [1 1 0] zone axis of a Ag-like fcc structure, respectively. Moreover, the presence of these planes evidences the crystallinity of the nanoparticles. In Fig. 1f, a faceted microstructure could be clearly seen in the HRTEM image of MBA-AgNPs. This structure has a fivefold symmetry around the [1 1 0] fcc axis with a quintuple twin ((1 1 1) fcc twinning plane). Moreover, these kinds of HRTEM images were simulated as Marks decahedra for Ag and other systems.[53,54] The Marks decahedron structure has 10 triangular {1 1 1} faces, 10 isosceles trapezoid {1 1 1} faces and 5 rectangular {1 0 0} faces. The simulation of the image shown in

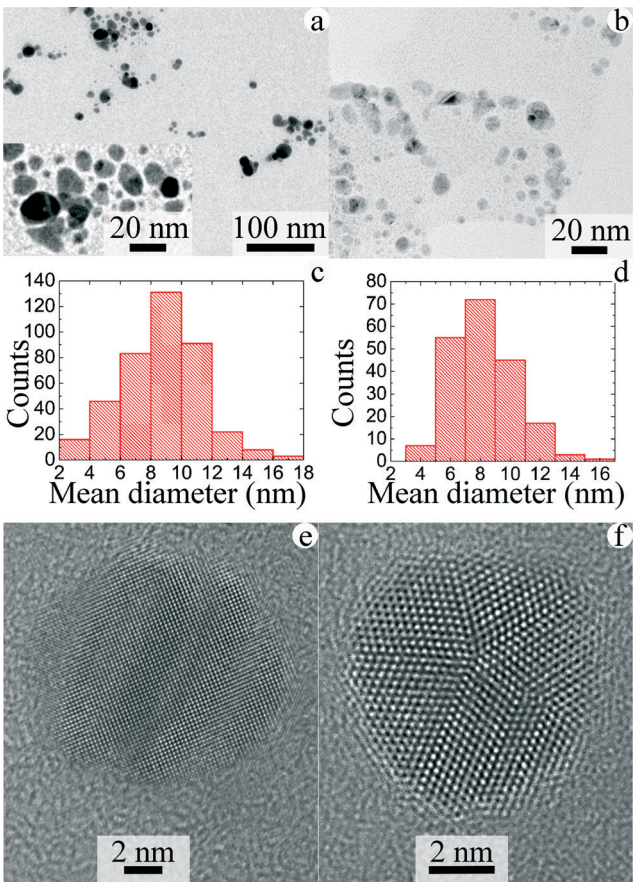

Fig. 1 TEM images, size distribution histograms and HRTEM images of CIT-AgNPs [(a), (c) and (e)] and of MBA-AgNPs [(b), (d) and (f)].

Fig. 1f involved more than 70% of the surface atoms over {1 1 1} faces (Fig. S6 in the ESI†).

A high resolution XPS spectrum of MBA-AgNPs in the S 2p region is shown in Fig. 2a. The S 2p region can be fitted with a principal component at S $2p_{3/2}$ BE ≈ 162.5 eV (red curve) assigned to a thiolate–Ag bond and another much smaller peak at 163.8 eV (blue curve) due to non-chemisorbed MBA molecules.[54,55] The ratio (r) of the integrated area of the 162 eV S 2p peak area and that of the Ag 3d is a measure of thiolate coverage on the AgNP surface. A value of r = 0.50–0.53 is obtained, which is in accordance with MBA-AgNPs suspended in alkaline media.[54] The existence of the thiolate–Ag bond implies that the carboxylic groups of MBA are exposed to the outer part of the AgNP interface, giving the possibility that depending on the pH (MBA on Ag pK_a = 5.8–6.0 (ref. 42, 56 and 57)) the negatively charged carboxylate moiety should play an important role, in particular considering the different forces that will take place at the interface AgNPs/phospholipid monolayer. The C 1s region can be fitted with four components: the 284.7–284.9 eV peak assigned to C bonded to H and C (orange line), another at 286.1–286.4 eV (turquoise line) due to C–COOH and C–OH (in CIT-AgNPs) and the contribution of the COO^- and COOH at 288.4–288.6 eV (fuchsia line) and 289.8–290.6 eV (green line), respectively.[57–59]

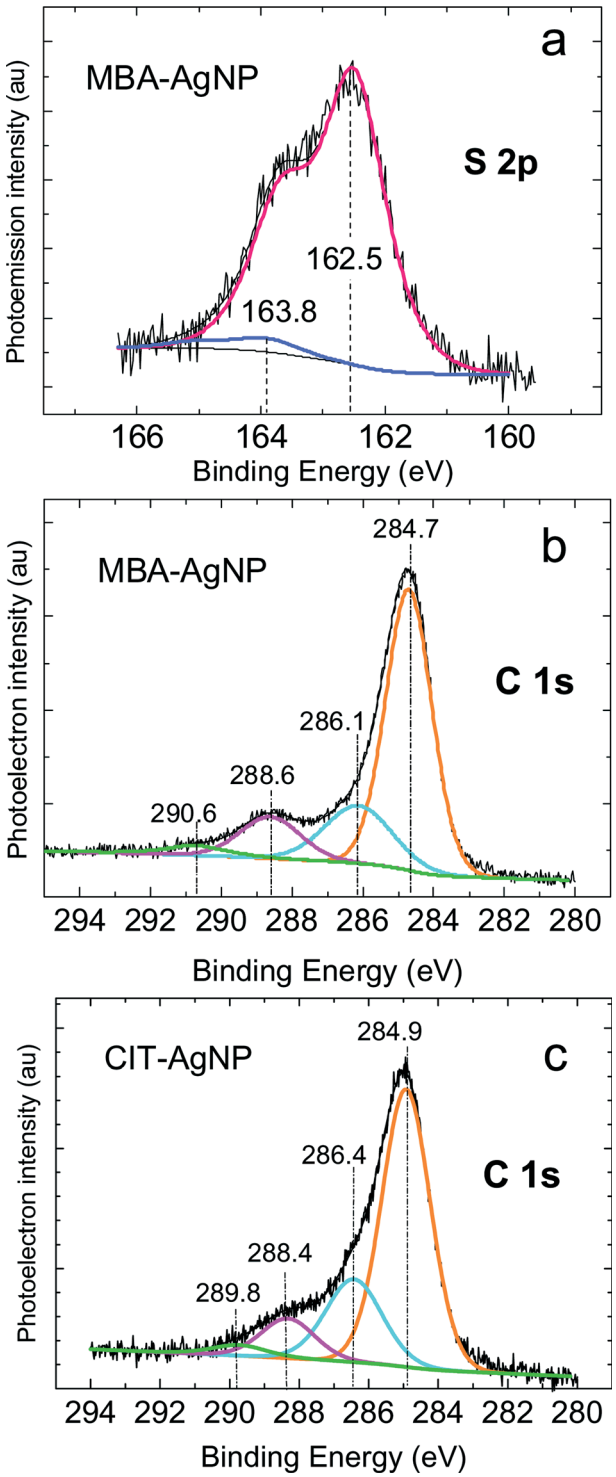

Fig. 2 XPS spectra of Ag nanoparticles capped with MBA (a and b) and CIT (c). In a) the fitting gives two components: one corresponding to thiolate–Ag bond molecules (red line) and the other at higher binding energies, corresponding to physisorbed thiols (blue).

Interesting data emerge from quantitative analysis of the surface components of AgNPs (Table 1).

In MBA-AgNPs, the COO_{tot}/S atomic ratio should be 1 according to the MBA molecular formula instead of the experimental value 0.75/051 = 1.47. Taking into account the attenuation of the electrons emitted by S due to the effective thickness of the molecule,[60] the corrected S_{total}/Ag ratio is 0.51/0.88 = 0.58, and therefore COO_{tot}/S = 1.34. There is still an excess of carboxylic groups with respect to S according to the molecular formula. This could be due to the incomplete ligand exchange reaction of citrate anions with MBA that leads to a complex capping layer formed by both molecules, as was proposed for Au nanoparticles.[61–63] Thus, the MBA-AgNPs have a capping layer composed of both MBA and citrate molecules in a molecular ratio MBA/CIT ≅ 6 (see calculation details in the ESI†)

For CIT-AgNPs, the 0.26 atomic ratio for COO/Ag is three times lower than that in the thiolated AgNPs (0.75), which is a relevant point to interpret their behavior when the interactions of either CIT-AgNPs or MBA-AgNPs with phospholipid monolayers are analyzed in the following section.

Adsorption of CIT-AgNPs and MBA-AgNPs at the interface of DMPC monolayers

We studied the interactions of two negatively charged silver nanoparticles that have the same core size and very similar

Table 1 Atomic ratio obtained from XPS spectra of MBA-AgNPs and CIT-AgNPs

	COO_{tot}/Ag[a]	S_{total}/Ag
MBA-AgNPs	0.75	0.51
CIT-AgNPs	0.26	—

[a] COO_{tot} corresponds to the sum of COO^- and COOH contributions.

sectional area upon functionalization with citrate or MBA, as shown before in Fig. 1, with DMPC Langmuir monolayers. Also, both AgNPs have almost the same zeta potential value (−36 mV for MBA-AgNPs and −33 mV for CIT-AgNPs) in the buffer solution where these measurements were performed. The zeta potential reflects the electrostatic potential at the electrical double layer surrounding a nanoparticle in solution and is related to the surface charge of the nanoparticle.[64] However, the chemical nature of the adsorbed citrate for CIT-AgNPs (aliphatic) and of mercaptobenzoic acid (aromatic moiety) for MBA-AgNPs should be taken into account, as well as the coverage and configuration of these molecules on the AgNP surface.

We studied the interactions of both CIT-AgNPs and MBA-AgNPs with DMPC monolayers at different initial surface pressures, which involve different initial surface packings of the phospholipid molecules at the interface. Once the DMPC lateral pressure is established, we analyze the effect of injecting a certain concentration of nanoparticles into the subphase, trying to mimic what would occur in real systems where cell membranes of living organisms are exposed to nanoparticles that can alter their structure and equilibrium properties. The attachment of particles to fluid interfaces is a complex process affected by a broad range of physicochemical parameters such as nanoparticle size, chemical nature of capping molecules, surface roughness, and wettability.[65,66] The total energy involved in the attachment of particles to a fluid interface depends on the difference between the energies of the particle at the interface and in the colloidal solution. Particles of micrometric size are usually irreversibly attached to fluid interfaces whereas for nanoparticles the reversibility of the adsorption can be regulated by modification of the contact angle.[66] Law and colleagues pointed out that the attachment to the interface of particles larger than 10 nm can be considered completely irreversible. However, for nanoparticles with radii smaller than 10 nm, a true thermodynamic equilibrium between the bulk solution and the interface is established.[67]

The interaction of CIT-AgNPs and MBA-AgNPs with the model biomembranes was characterized by means of surface pressure changes ($\Delta\pi = f(t)$) as a function of time (at a constant surface area) and by the inspection of the compression isotherms measured after the interaction/adsorption occurs. Although the observed changes in surface pressure ($\Delta\pi$) were small, we found that the magnitude and the range of lateral phospholipid pressures where the interactions occur depend on the initial surface packing of DMPC and on the capping molecule.

To perform these experiments, the lipid monolayer of DMPC was first formed by spreading a solution of DMPC (in chloroform) at the air/buffer interface (at a fixed surface area). Once the desired surface pressure for DMPC (π_o^{DMPC}) was reached and kept constant for 10 min, a volume of 1.5 mL of AgNP solution was injected into the subphase, and the surface pressure was measured until its stabilization ($\pi_f^{DMPC+AgNPs}$). After that, the area of the trough was reduced and the compression isotherm was obtained. The change in surface pressure ($\Delta\pi$) was calculated as shown in eqn (3); the values obtained for $\Delta\pi$ are shown in Table 2, and the adsorption isotherms are shown in Fig. 3 and S7.†

$$\Delta\pi = \left(\pi_f^{DMPC+AgNPs}\right) - \left(\pi_o^{DMPC}\right) \quad (3)$$

By examining the relationship between $\Delta\pi$ and π_o^{DMPC}, it is seen that CIT-AgNPs and MBA-AgNPs interact more favorably with DMPC when the monolayer is packed at 5 mN m^{-1} and $\Delta\pi$ is of the same order for both CIT-AgNPs and MBA-AgNPs. For higher initial pressures of DMPC (π_o^{DMPC}), the AgNPs in the subphase cause negligible changes in π, indicating that a certain degree of packing or organization of the DMPC layer is necessary in order that nanoparticles could be inserted in or adsorbed on the interface, as has been proposed previously.[68] It should be noted that the surface pressure interval between 30 and 35 mN m^{-1} in a monolayer is proposed to offer an organization with comparable compressibility to that mostly found in natural biomembranes.[69] Nevertheless, the behavior of natural membranes is dynamic, and lower lateral pressures should be taken into account in the evaluation of interactions at the interface.[70]

Then we select $\pi_o^{DMPC} \cong 5$ mN m^{-1} to explore the dependence of the interactions between CIT-AgNPs/DMPC and MBA-AgNPs/DMPC when the DMPC layer is compressed after the interaction with the NPs (Fig. 4a and b). Upon inspection of the compression isotherms, it can be seen that CIT-AgNPs and MBA-AgNPs modify the area occupied by DMPC when compared with the area obtained for the pure phospholipid monolayer in contact with the buffer subphase.

Citrate modified silver nanoparticles change the surface area occupied by DMPC up to a pressure of about 35–40 mN m^{-1} (Fig. 4a). Higher compression results in the overlap of both isotherms until collapse, indicating the expulsion of the CIT-AgNPs from the interface. The expulsion of nanoparticles interacting with a zwitterionic phospholipid monolayer was also observed for negatively charged silica nanoparticles (diameter, 30 nm; zeta potential, −42 mV)[71] and citrate capped gold nanoparticles (diameter, 17 nm; zeta potential, −56 mV).[34]

On the contrary, for MBA-AgNPs the shift in area relative to that occupied by DMPC is maintained along the whole compression of the film (Fig. 4b). The surface compressional modulus C_s^{-1} was calculated according to eqn (4).[45] This parameter is an important characteristic of the monolayer related to its rigidity and to the capability to store elastic energy.[33]

$$C_s^{-1} = -A\left(\frac{d\pi}{dA}\right)_T \quad (4)$$

A represents the total monolayer area and is obtained from the Langmuir isotherms. At low surface pressures, CIT-AgNPs induce a decrease of C_s^{-1} which implies a lower rigidity of the film compared to pure DMPC. This trend is

Table 2 Changes in surface pressure ($\Delta\pi$) produced by the interaction of CIT-AgNPs and MBA-AgNPs with DMPC monolayers packed at different initial surface pressures (π_o)[a]

π_o (mN m^{-1}) DMPC	$\Delta\pi$ (mN m^{-1}) CIT-AgNPs/DMPC	π_o (mN m^{-1}) DMPC	$\Delta\pi$ (mN m^{-1}) MBA-AgNPs/DMPC
3.5	1.79	—	—
5.2	3.40	5.7	3.42
10.3	1.10	10.5	2.38
33.6	0.50	30	0

[a] The subphase was a pH 7.2 phosphate buffer solution, T: 23 ± 1 °C. For MBA-AgNPs, the experiments were done for $\pi_o \geq 5$ mN m^{-1}.

observed until an area of about 80–82 Å^2. After this packing area, no changes in C_s^{-1} of the CIT-AgNPs/DMPC system was observed with respect to buffer/DMPC, pointing out that the CIT-AgNPs did not significantly modify the surface elasticity of the film, as shown in Fig. 4c. However, for MBA-AgNPs/DMPC an increase in C_s^{-1} indicates a decrease in the film elasticity due to the interaction of the DMPC monolayer with MBA-AgNPs (Fig. 4d).

An interesting fact emerges when only citrate or 4-mercaptobenzoic acid molecules (not forming part of the capping of AgNPs) are dissolved in the subphase solution in contact with DMPC, since no shift was observed and both isotherms were superposed (Fig. S8†). This reflects the difficulty of transferring citrate or MBA ions from the aqueous to the lipid phase, contrary to that observed for both CIT-AgNPs and MBA-AgNPs (Fig. 4a and b). The electrostatic component of the Gibbs energy given by the Born expression[72] (eqn (5)) can justify the higher energy required for the smaller radius ions (with charge q), compared to the energy required when the ions form part of the NPs as capping agents, to transfer from the aqueous phase to the hydrophobic lipid layer with dielectric constants ε_w and ε_M, respectively.

$$\Delta G_{Born} = -\frac{q^2}{8\pi\varepsilon_0 r}\left(\frac{1}{\varepsilon_w} - \frac{1}{\varepsilon_m}\right) \quad (5)$$

Thus, the changes in surface pressure observed in Fig. 4a and b could only be attributed to the ensemble CIT-AgNPs or MBA-AgNPs. It has been reported previously that for MBA and MUA (mercaptoundecanoic acid) functionalized Au surfaces, the aromatic layer binds higher amounts of the protein BSA than the aliphatic one.[57] A possible explanation is the high electronic density provided by the aromatic ring that favors van der Waals forces with the hydrocarbon chains of DMPC.

Thus, we should explain why both AgNPs having carboxylate terminal groups and similar zeta potentials exposed to the DMPC have the same interaction behavior up to 35–40 mN m^{-1} and why MBA-AgNPs are not excluded from the interface at higher surface pressures. Since both CIT-AgNPs and MBA-AgNPs have carboxylate terminal groups with a negative charge at the pH of the experiments, one may infer that at $\pi_o^{DMPC} \cong 5$ mN m^{-1}, a value where both CIT-AgNPs and

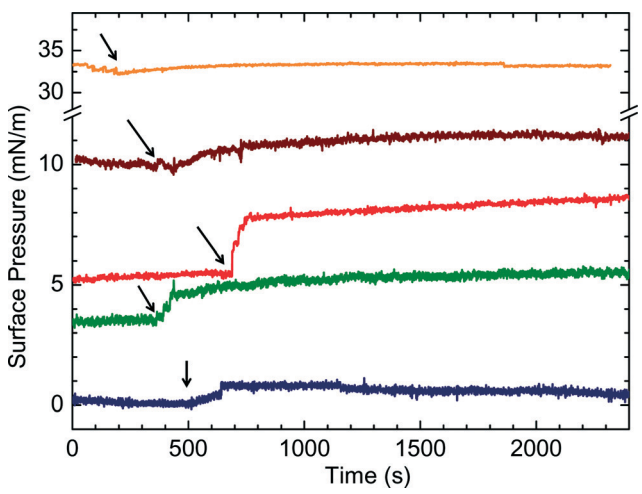

Fig. 3 Adsorption isotherms of CIT-AgNPs in the absence (blue curve) and in the presence of a DMPC monolayer initially packed at π_o^{DMPC} = 3 mN m^{-1} (green), 5 mN m^{-1} (red), 10 mN m^{-1} (brown) and 33 mN m^{-1} (orange). The arrows indicate the moment when AgNPs are injected.

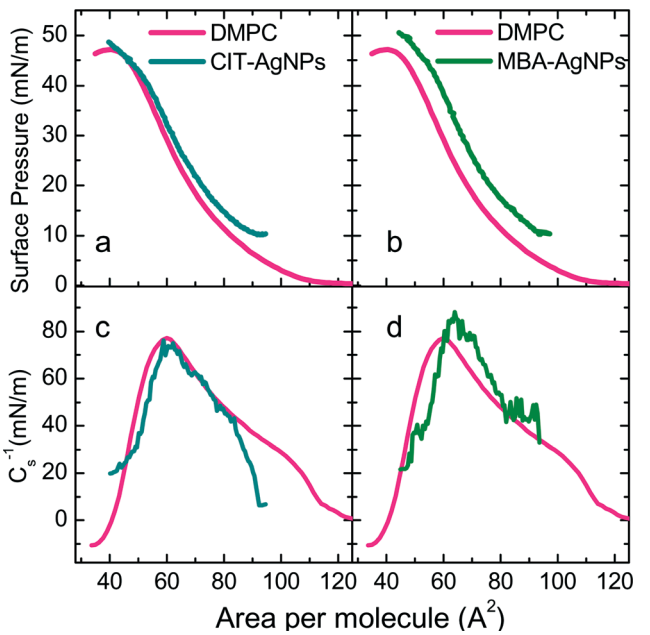

Fig. 4 Compression isotherms (a, b) and surface compressional modulus C_s^{-1} (c, d) obtained for CIT-AgNPs (a, c) and MBA-AgNPs (b, d) adsorbed on a DMPC monolayer initially packed at 5 mN m^{-1}.

MBA-AgNPs produce the same effect on the surface pressure, the predominant interaction is mainly due to attractive electrostatic forces with the positive charge of the N atom of the polar group of DMPC (Fig. S9†), as has been proposed for interactions between citrate functionalized Au,[51] Ag (ref. 73) and hydrophilic silica nanoparticles interacting with DPPC.[34,74] At $\pi_o^{DMPC} \cong 5$ mN m^{-1}, both CIT-AgNPs and MBA-AgNPs are adsorbed on or partially inserted in the DMPC layer, expanding the surface area. When the compression proceeds, the lateral force favors a higher packing of DMPC molecules, optimizing their van der Waals forces that become more important than the electrostatic interactions with CIT-AgNPs, and the behavior of pure DMPC is recovered (Fig. 4a).

The topography of the interface from the air side was visualized by BAM. A series of images from the initial time of the injection of NPs into the subphase up to *ca.* 110 min are shown in Fig. 5. In this experiment, NPs are injected into the subphase in a Langmuir trough where DMPC is equilibrated at $\pi_o^{DMPC} = 5$ mN m^{-1}. Images for the pure buffer and DMPC (shown in the first two images of both sequences) exhibit a homogeneous topography, and no changes were observed over periods of time comparable to those of the following images that correspond to buffer solutions containing Ag nanoparticles. Along 110 min, few bright spots appear at the interface, indicating that both CIT-AgNPs and MBA-AgNPs interact with the phospholipid, as shown in Fig. 5 and S10.† This result is in agreement with the adsorption isotherms and compression isotherms described previously. Taking into account all the experimental evidence, the general trend shows that these nanoparticles interact with the polar head lipid group without being completely inserted in or penetrating through the lipid monolayer. Nevertheless, they remain adsorbed at the interface, perturbing or modifying the phospholipid packing (as shown by the isotherms), which may have strong implications in their toxicological effects considering that their degradation produces silver ions[73,75,76] whose diffusion would be facilitated taking into account the expansion and disorder of the lipid layer caused by the AgNP adsorption/insertion. Silver ions could participate in the formation of reactive oxygen species (ROS) that promote oxidative reactions in the cell membrane and inside the cell in living organisms.[77]

Now, the question about the nature of the physicochemical forces that permit the permanence of MBA-AgNPs along all pressures arises, a fact that points out that there is another component which allows a stronger interaction. This could be higher electrostatic interactions of MBA-AgNPs compared with CIT-AgNPs and/or hydrophobic forces between MBA-AgNPs and the hydrocarbon tails of DMPC.

Surface structure of citrate and MBA adsorbed on AgNPs

XPS data (Table 1) show that the atomic ratio of carboxylic groups in MBA-AgNPs is three times higher than that in CIT-AgNPs. Our previous data on the adsorption of 4-mercaptobenzoic acid on Ag surfaces indicate that MBA is adsorbed on Ag through a thiolate bond exposing the carboxylate groups to the external part of the interface (Fig. S11†).[54] In the case of CIT-AgNPs, considering that citrate contains three carboxylate groups per molecule, the question arises as to which of them are involved in the adsorption on Ag and which are exposed to the solution and are capable of interacting with the polar groups of DMPC monolayers.

DFT calculations were employed to explore the energetic and structural characteristics of citrate adsorption on Ag (1 1 1) since this plane is relevant for the AgNPs, as demonstrated by the HRTEM images. A rough estimation using a Marks model to simulate the HRTEM images gives more than 73% of the metallic atoms lying on the {1 1 1} faces and the remaining on the {1 0 0} faces (Fig. S6†).

The optimized surface structure of citrate on Ag (1 1 1) is shown in Fig. 6, and the structural and energetic parameters obtained for that configuration are listed in Table 3. The citrate radical was adsorbed on the Ag (1 1 1) surface

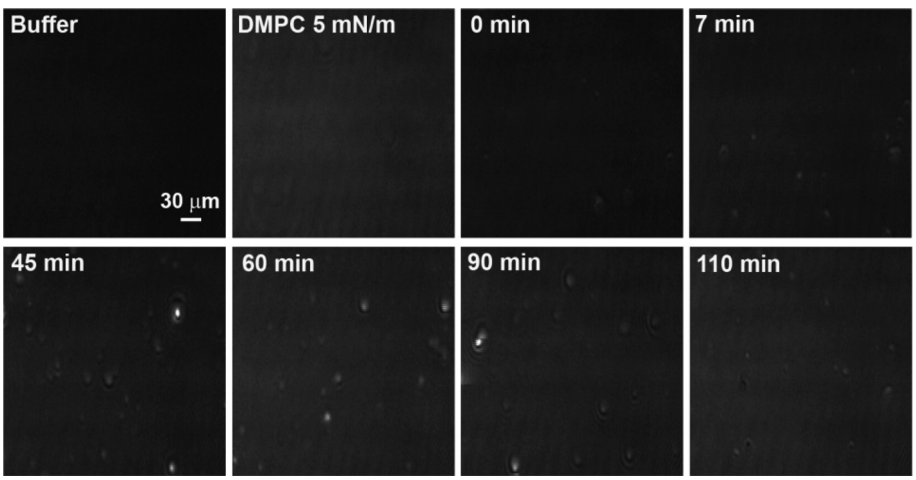

Fig. 5 Time sequence of BAM images taken for a DMPC monolayer film at 5 mN m^{-1} in contact with phosphate buffer solution at pH 7.2 containing CIT-AgNPs.

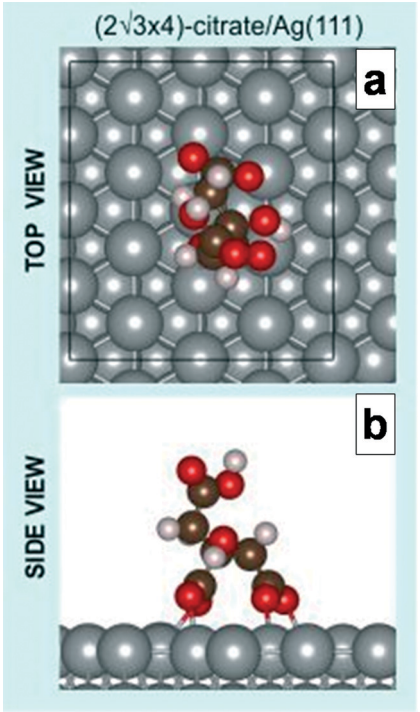

Fig. 6 Optimized structure for citrate (CIT) on Ag (1 1 1). Grey: Ag. Brown: C. Red: O. White: H.

Table 3 Coverage (θ), average binding energy (E_b), Gibbs free energy of adsorption (γ) and Ag–O distance for citrate (CIT) on Ag (1 1 1)

Surface lattice	$(2\sqrt{3} \times 4)$
θ	0.063
E_b/eV	−1.44
γ/meV Å^{-2}	−12.12
d(Ag–O)/Å	2.28

configuration *via* the terminal and central η_2-COO^- groups with a free COOH group exposed to the solution.

The experimental XPS COO_{Tot}/Ag atomic ratio (r) for CIT-AgNPs was 0.26, which implies that this ratio for citrate molecules is ≅0.09 (three carboxylic groups per molecule). The configuration predicted by DFT calculations shows that two carboxylates are involved in the adsorption on the Ag surface and the other carboxylic moiety is exposed to the outer part of the interface (Fig. 6, side view). The experimental XPS COO_{Tot}/Ag atomic ratio for MBA-AgNPs was 0.76, more than eight times higher than that corresponding to the carboxylate group exposed to the interface for CIT-AgNPs (0.09). Thus, one may infer that at the beginning of the compression experiment, after the AgNPs interacted with DMPC packed at 5 mN m^{-1}, the carboxylate groups in both CIT-AgNPs and MBA-AgNPs interact in the same way with the ammonium of the polar head group of DMPC that adopts a configuration where the monolayer is 10–15% more expanded than in the absence of AgNPs in the subphase. When the compression proceeds, CIT-AgNPs are excluded due to weaker electrostatic interactions compared with MBA-AgNPs that remain at the interface until the collapse of the monolayer. Experiments with liposomes done with different types of lipids showed that the local phase change seemed to depend on the density and placement of charges on the surface of the nanoparticles; nanoparticles with a higher density of surface charge induce structural reorganization of the lipids and modify their local state.[25,78] The chemical nature of citrate or 4-mercaptobenzoic acid is not responsible for the changes in surface pressure observed in Fig. 4a and b, which could only be attributed to the ensemble CIT-AgNPs or MBA-AgNPs. The fact that nanoparticles with similar zeta potentials and different ligand shell structures such as our AgNPs have different behaviors in their interaction with membranes has also been observed for gold nanoparticles in their interaction with cells.[79] Our experimental evidence and theoretical calculations suggest that what plays a fundamental role, and probably defines the type and magnitude of interactions established, is the surface charge density on the NP surface rather than the macroscopic zeta potential.

In addition, hydrophobic interactions of the aromatic ring of MBA with the hydrocarbon chain of DMPC could play a role in favoring the anchorage of AgNPs. Atomistic molecular dynamic simulations showed a pathway where a single hydrophobic NP ligand anchors the nanoparticle to the bilayer, allowing a close contact with the membrane surface until lipid protrusion occurs and facilitating insertion.[80] A fixed nanoparticle at the interface increases the emergence of tail protrusions, lowering the barrier for the insertion of additional nanoparticles as in a nucleation-and-growth kinetic process.[81] It should also be taken into account that hydrophobic interactions depend on the radius (r) as $1/r^6$, whereas electrostatic forces vary with $1/r$. Thus, in MBA-AgNPs, the synergy of both long-range (hydrophobic) and short-range (electrostatic) forces contributes to stabilizing their permanence at the interface and is responsible for the difference with CIT-AgNPs in the interactions with DMPC reflected in their compression isotherms.

Conclusions

Two negatively charged silver nanoparticles that have the same core size and very similar sectional area upon functionalization with citrate or 4-mercaptobenzoic acid follow two regimes in their interactions with DMPC Langmuir monolayers. At low surface pressures, both types of AgNPs interact in a similar way, expanding the phospholipid molecular area. Upon compression, CIT-AgNPs are excluded from the interface, whereas MBA-AgNPs remain adsorbed. Neither penetration nor changes in the reflectivity of DMPC were observed from Brewster angle images, which points out that the interaction is confined to the AgNP/DMPC interface.

XPS results and DFT calculations show a higher density of carboxylate anions in MBA-AgNPs than in CIT-AgNPs. The absence of expansion of DMPC in the presence of either MBA or citrate solutions confirms that the ensemble of these

molecules with AgNPs is needed to distort the phospholipid monolayer. We propose that the permanence of MBA-AgNPs in all the range of surface pressures may be interpreted on the basis of their higher electrostatic interactions with the positive ammonium moiety of the polar end of DMPC and on the hydrophobic interactions mediated by the aromatic groups with lipid tail protrusions of the phospholipids or at phospholipid monolayer defects where the aromatic ring/hydrocarbon chain proximity is favored. These results highlight the importance of understanding, at the molecular level, the interactions between nanomaterials and membranes to assess their potential long-term toxicological effects.

Acknowledgements

We acknowledge financial support from ANPCyT (PICT 2010-2554, 2012-1808 and 2013-1175) and CTQ2011-24784, Spain. P. C. thankfully acknowledges the computer resources provided by the Computer Support Service for Research (SAII) at La Laguna University. JVMG is a CONICET fellow. MEV is a researcher from CIC Buenos Aires. R. V. V. and B. M. are Career Investigators of CONICET-UNC. The authors thank Dr. Julio Azcárate for useful discussions about the surface chemistry of AgNPs. EZ is Career Investigator of CONICET.

References

1 S. Foss Hansen, L. R. Heggelund, P. Revilla Besora, A. Mackevica, A. Boldrin and A. Baun, *Environ. Sci.: Nano*, 2016, **3**, 169–180.
2 Global Market for Nano Silver, Accessed http://www.researchandmarkets.com/publication/mz9dqee/global_silver_nanoparticles_market_20152019.
3 S. W. P. Wijnhoven, W. J. G. M. Peijnenburg, C. A. Herberts, W. I. Hagens, A. G. Oomen, E. H. W. Heugens, B. Roszek, J. Bisschops, I. Gosens, D. Van de Meent, S. Dekkers, W. H. De Jong, M. Van Zijverden, A. J. A. M. Sips and R. E. Geertsma, *Nanotoxicology*, 2009, **3**, 109–138.
4 J. R. Morones, J. L. Elechiguerra, A. Camacho, K. Holt, J. Kouri, B. J. Tapia Ramírez and M. J. Yacaman, *Nanotechnology*, 2005, **16**, 2346.
5 C.-C. Li, S.-J. Chang, F.-J. Su, S.-W. Lin and Y.-C. Chou, *Colloids Surf., A*, 2013, **419**, 209–215.
6 Y. Sun, *Chem. Soc. Rev.*, 2013, **42**, 2497–2511.
7 N. L. Pacioni, C. D. Borsarelli, V. Rey and A. V. Veglia, in *Silver Nanoparticle Applications*, ed. E. I. Alarcon, M. Griffith and K. I. Udekwu, Springer International Publishing, 2015, ch. 2, pp. 13–46.
8 J. Turkevich, P. C. Stevenson and J. Hillier, *Faraday Discuss. Chem. Soc.*, 1951, **11**, 55–75.
9 A. Henglein and M. Giersig, *J. Phys. Chem. B*, 1999, **103**, 9533–9539.
10 M. Rycenga, C. M. Cobley, J. Zeng, W. Li, C. H. Moran, Q. Zhang, D. Qin and Y. Xia, *Chem. Rev.*, 2011, **111**, 3669–3712.
11 K. G. Stamplecoskie, J. C. Scaiano, V. S. Tiwari and H. Anis, *J. Phys. Chem. C*, 2011, **115**, 1403–1409.
12 T. Quang Huy, N. Van Quy and L. Anh-Tuan, *Adv. Nat. Sci.: Nanosci. Nanotechnol.*, 2013, **4**, 033001.
13 H. J. Johnston, G. Hutchison, F. M. Christensen, S. Peters, S. Hankin and V. Stone, *Crit. Rev. Toxicol.*, 2010, **40**, 328–346.
14 A. E. Nel, L. Madler, D. Velegol, T. Xia, E. M. V. Hoek, P. Somasundaran, F. Klaessig, V. Castranova and M. Thompson, *Nat. Mater.*, 2009, **8**, 543–557.
15 T.-H. Kim, M. Kim, H.-S. Park, U. S. Shin, M.-S. Gong and H.-W. Kim, *J. Biomed. Mater. Res., Part A*, 2012, **100A**, 1033–1043.
16 M. Mahmoudi, J. Meng, X. Xue, X. J. Liang, M. Rahman, C. Pfeiffer, R. Hartmann, P. R. Gil, B. Pelaz, W. J. Parak, P. del Pino, S. Carregal-Romero, A. G. Kanaras and S. Tamil Selvan, *Biotechnol. Adv.*, 2014, **32**, 679–692.
17 Q. Mu, G. Jiang, L. Chen, H. Zhou, D. Fourches, A. Tropsha and B. Yan, *Chem. Rev.*, 2014, **114**, 7740–7781.
18 A. Verma and F. Stellacci, *Small*, 2010, **6**, 12–21.
19 B. Baroli, M. G. Ennas, F. Loffredo, M. Isola, R. Pinna and M. A. Lopez-Quintela, *J. Invest. Dermatol.*, 2007, **127**, 1701–1712.
20 L. Shang, K. Nienhaus and G. Nienhaus, *J. Nanobiotechnol.*, 2014, **12**, 5.
21 E. A. K. Warren and C. K. Payne, *RSC Adv.*, 2015, **5**, 13660–13666.
22 E. H. Shin, Y. Li, U. Kumar, H. V. Sureka, X. Zhang and C. K. Payne, *Nanoscale*, 2013, **5**, 5879–5886.
23 V. Kodali, M. H. Littke, S. C. Tilton, J. G. Teeguarden, L. Shi, C. W. Frevert, W. Wang, J. G. Pounds and B. D. Thrall, *ACS Nano*, 2013, **7**, 6997–7010.
24 R. C. Van Lehn, M. Ricci, P. H. J. Silva, P. Andreozzi, J. Reguera, K. Voïtchovsky, F. Stellacci and A. Alexander-Katz, *Nat. Commun.*, 2014, 5.
25 B. Wang, L. Zhang, S. C. Bae and S. Granick, *Proc. Natl. Acad. Sci. U. S. A.*, 2008, **105**, 18171–18175.
26 J. Lin, H. Zhang, Z. Chen and Y. Zheng, *ACS Nano*, 2010, **4**, 5421–5429.
27 C. M. Goodman, C. D. McCusker, T. Yilmaz and V. M. Rotello, *Bioconjugate Chem.*, 2004, **15**, 897–900.
28 E. C. Cho, J. Xie, P. A. Wurm and Y. Xia, *Nano Lett.*, 2009, **9**, 1080–1084.
29 A. P. Girard-Egrot and L. J. Blum, in *Nanobiotechnology of Biomimetic Membranes*, ed. D. K. Martin, Springer, New York, 2007, ch. 2, pp. 23–74.
30 S. Tatur and A. Badia, *Langmuir*, 2012, **28**, 628–639.
31 S. Tatur, M. Maccarini, R. Barker, A. Nelson and G. Fragneto, *Langmuir*, 2013, **29**, 6606–6614.
32 J. M. Troiano, L. L. Olenick, T. R. Kuech, E. S. Melby, D. Hu, S. E. Lohse, A. C. Mensch, M. Dogangun, A. M. Vartanian, M. D. Torelli, E. Ehimiaghe, S. R. Walter, L. Fu, C. R. Anderton, Z. Zhu, H. Wang, G. Orr, C. J. Murphy, R. J. Hamers, J. A. Pedersen and F. M. Geiger, *J. Phys. Chem. C*, 2015, **119**, 534–546.
33 E. Guzmán, L. Liggieri, E. Santini, M. Ferrari and F. Ravera, *J. Phys. Chem. C*, 2011, **115**, 21715–21722.
34 A. A. Torrano, Â. S. Pereira, O. N. Oliveira Jr. and A. Barros-Timmons, *Colloids Surf., B*, 2013, **108**, 120–126.

35 S. S. You, R. Rashkov, P. Kanjanaboos, I. Calderon, M. Meron, H. M. Jaeger and B. Lin, *Langmuir*, 2013, **29**, 11751–11757.

36 T. J. Matshaya, A. E. Lanterna, A. M. Granados, R. W. M. Krause, B. Maggio and R. V. Vico, *Langmuir*, 2014, **30**, 5888–5896.

37 A. Pallaoro, G. B. Braun, N. O. Reich and M. Moskovits, *Small*, 2010, **6**, 618–622.

38 C. E. Talley, L. Jusinski, C. W. Hollars, S. M. Lane and T. Huser, *Anal. Chem.*, 2004, **76**, 7064–7068.

39 J. Kneipp, H. Kneipp and K. Kneipp, *Chem. Soc. Rev.*, 2008, **37**, 1052–1060.

40 J. Kneipp, H. Kneipp, B. Wittig and K. Kneipp, *J. Phys. Chem. C*, 2010, **114**, 7421–7426.

41 J. Scaffidi, M. Gregas, V. Seewaldt and T. Vo-Dinh, *Anal. Bioanal. Chem.*, 2009, **393**, 1135–1141.

42 F. Wang, R. G. Widejko, Z. Yang, K. T. Nguyen, H. Chen, L. P. Fernando, K. A. Christensen and J. N. Anker, *Anal. Chem.*, 2012, **84**, 8013–8019.

43 E.-D. Raghda, G. Mariam and M. E. A. Hassan, in *Functional Nanoparticles for Bioanalysis, Nanomedicine, and Bioelectronic Devices Volume 1*, American Chemical Society, 2012, ch. 14, vol. 1112, pp. 359–404.

44 X. Han, H. Wang, X. Ou and X. Zhang, *ACS Appl. Mater. Interfaces*, 2013, **5**, 5811–5814.

45 G. L. Gaines, in *Interscience Monographs on Physical Chemistry*, ed. I. Prigogine, Wiley Interscience, New York, First edn, 1966.

46 G. Kresse and J. Hafner, *Phys. Rev. B: Condens. Matter Mater. Phys.*, 1993, **48**, 13115–13118.

47 G. Kresse and J. Furthmüller, *Comput. Mater. Sci.*, 1996, **6**, 15–50.

48 M. Dion, H. Rydberg, E. Schroder, D. C. Langreth and B. I. Lundqvist, *Phys. Rev. Lett.*, 2004, **92**, 246401.

49 J. Klimes, D. R. Bowler and A. Michaelides, *J. Phys.: Condens. Matter*, 2010, **22**, 074203–074203.

50 P. E. Blöchl, *Phys. Rev. B: Condens. Matter Mater. Phys.*, 1994, **50**, 17953–17979.

51 H. J. Monkhorst and J. D. Pack, *Phys. Rev. B: Solid State*, 1976, **13**, 5188–5192.

52 W. B. Pearson, *Handbook of Lattice Spacing and Structure of Metals*, Pergamon Press, Inc., New York, 1958.

53 C. Y. Tan, J. S. Chen, B. H. Liu and G. M. Chow, *J. Cryst. Growth*, 2006, **293**, 175–185.

54 J. V. Maya Girón, E. Zelaya, A. Rubert, G. Benítez, P. Carro, R. C. Salvarezza and M. E. Vela, *J. Phys. Chem. C*, 2013, **117**, 24967–24974.

55 F. Bensebaa, T. H. Ellis, E. Kruus, R. Voicu and Y. Zhou, *Langmuir*, 1998, **14**, 6579–6587.

56 S. W. Bishnoi, C. J. Rozell, C. S. Levin, M. K. Gheith, B. R. Johnson, D. H. Johnson and N. J. Halas, *Nano Lett.*, 2006, **6**, 1687–1692.

57 A. Vallée, V. Humblot, R. Al Housseiny, S. Boujday and C.-M. Pradier, *Colloids Surf., B*, 2013, **109**, 136–142.

58 R. Urcuyo, E. Cortés, A. A. Rubert, G. Benitez, M. L. Montero, N. G. Tognalli, A. Fainstein, M. E. Vela and R. C. Salvarezza, *J. Phys. Chem. C*, 2011, **115**, 24707–24717.

59 J.-W. Park and J. S. Shumaker-Parry, *J. Am. Chem. Soc.*, 2014, **136**, 1907–1921.

60 P. E. Laibinis, C. D. Bain and G. M. Whitesides, *J. Phys. Chem.*, 1991, **95**, 7017–7021.

61 S. Zhang, G. Leem, L.-o. Srisombat and T. R. Lee, *J. Am. Chem. Soc.*, 2008, **130**, 113–120.

62 J. Duan, M. J. Linman, C.-Y. Chen and Q. J. Cheng, *J. Am. Soc. Mass Spectrom.*, 2009, **20**, 1530–1539.

63 J.-W. Park and J. S. Shumaker-Parry, *ACS Nano*, 2015, **9**, 1665–1682.

64 J. D. Clogston and A. K. Patri, Zeta potential measurement, *Methods Mol. Biol.*, 2011, **697**, 63–70.

65 A. Maestro, E. Guzmán, F. Ortega and R. G. Rubio, *Curr. Opin. Colloid Interface Sci.*, 2014, **19**, 355–367.

66 A. Maestro, E. Santini, D. Zabiegaj, S. Llamas, F. Ravera, L. Liggieri, F. Ortega, R. G. Rubio and E. Guzman, *Adv. Condens. Matter Phys.*, 2015, **2015**, 17.

67 H. S. Wi, S. Cingarapu, K. J. Klabunde and B. M. Law, *Langmuir*, 2011, **27**, 9979–9984.

68 S. Dai, X. Zhang, Z. Du, Y. Huang and H. Dang, *Colloids Surf., B*, 2005, **42**, 21–28.

69 D. Marsh, *Biochim. Biophys. Acta, Rev. Biomembr.*, 1996, **1286**, 183–223.

70 H. T. McMahon and J. L. Gallop, *Nature*, 2005, **438**, 590–596.

71 E. Guzmán, L. Liggieri, E. Santini, M. Ferrari and F. Ravera, *Colloids Surf., A*, 2012, **413**, 280–287.

72 A. G. Volkov and T. Hampton, in *Advances in Planar Lipid Bilayers and Liposomes*, ed. A. L. Liu, Academic Press, 2008, ch. 5, vol. 8, pp. 155–199.

73 L. B. Fen, S. Chen, Y. Kyo, K.-L. Herpoldt, N. J. Terrill, I. E. Dunlop, D. S. McPhail, M. S. Shaffer, S. Schwander, A. Gow, J. Zhang, K. F. Chung, T. D. Tetley, A. E. Porter and M. P. Ryan, *Environ. Sci. Technol.*, 2013, **47**, 11232–11240.

74 E. Guzmán, L. Liggieri, E. Santini, M. Ferrari and F. Ravera, *Colloids Surf., A*, 2012, **413**, 174–183.

75 R. Sridhar, K. Madhaiyan, S. Sundarrajan, A. Gora, J. R. Venugopal and S. Ramakrishna, *J. Mater. Chem. B*, 2014, **2**, 1626–1633.

76 P. Pallavicini, A. Taglietti, G. Dacarro, Y. Antonio Diaz-Fernandez, M. Galli, P. Grisoli, M. Patrini, G. Santucci De Magistris and R. Zanoni, *J. Colloid Interface Sci.*, 2010, **350**, 110–116.

77 R. M. Cordeiro, *Biochim. Biophys. Acta*, 2014, **1838**, 438–444.

78 K. A. Dawson, A. Salvati and I. Lynch, *Nat. Nanotechnol.*, 2009, **4**, 84–85.

79 A. Verma, O. Uzun, Y. Hu, Y. Hu, H.-S. Han, N. Watson, S. Chen, D. J. Irvine and F. Stellacci, *Nat. Mater.*, 2008, **7**, 588–595.

80 R. C. Van Lehn and A. Alexander-Katz, *Soft Matter*, 2015, **11**, 3165–3175.

81 R. C. Van Lehn and A. Alexander-Katz, *J. Phys. Chem. B*, 2014, **118**, 12586–12598.

